PAPER • OPEN ACCESS

DECAF cross-device characterization of tokamak disruptions indicated by abnormalities in plasma vertical position and current

OPEN ACCESS
IOP Publishing | International Atomic Energy Agency
Nuclear Fusion
Nucl. Fusion **64** (2024) 066030 (13pp)
https://doi.org/10.1088/1741-4326/ad3fca

DECAF cross-device characterization of tokamak disruptions indicated by abnormalities in plasma vertical position and current

V. Zamkovska[1,*], S.A. Sabbagh[1], M. Tobin[1], J.W. Berkery[2], J.D. Riquezes[1], Y.S. Park[3], K. Erickson[2], J. Butt[4], J.G. Bak[3], J. Kim[3], K.D. Lee[3], J. Ko[3], S.W. Yoon[3], C.J. Ham[5], L. Kogan[5] and the MAST Upgrade Team[a]

[1] Department of Applied Physics and Applied Mathematics, Columbia University, 500 W. 120th St, New York, NY 10027, United States of America
[2] Princeton Plasma Physics Laboratory, 100 Stellarator Road, Princeton, NJ 08540, United States of America
[3] Korea Institute of Fusion Energy, 169-148 Gwahak-ro, Yuseong-gu, Daejeon 34133, Korea, Republic Of
[4] Mechanical and Aerospace Engineering, Princeton University, Princeton, NJ 08544, United States of America
[5] United Kingdom Atomic Energy Authority, Culham Science Centre, Abingdon OX14 3DB, Oxfordshire, United Kingdom of Great Britain and Northern Ireland

E-mail: vk2475@columbia.edu

Received 23 January 2024, revised 20 March 2024
Accepted for publication 17 April 2024
Published 13 May 2024

Abstract

Abnormal (deviating from the target) variations in the plasma vertical position Z and current I_p (such as vertical displacements, transient I_p 'spikes' and quenches) constitute common elements of a disruption, a phenomenon that is to be mitigated, or ultimately avoided in future reactor-relevant tokamaks. While these abnormalities are generally recognized cross-shot and cross-device, details in terms of appearance (or not) and order of these abnormalities in disruption event chains (DEC) are bound to the plasma state at the time of the chain initiation. Detection of these abnormalities is thus indicative not only of the onset of the plasma collapse itself but also of the disruption driving cause that is promoted at a particular plasma state. Here, the occurrence of disruptions, explored via the detection of an I_p quench, and the analysis of DEC constituted by I_p and Z abnormalities is reported for in total seven full device-year pairs of operation of three machines (4, 2 and 1 years of KSTAR, MAST-U and NSTX-U operation, respectively) using the DECAF code expanded tools and capabilities. It is shown that the disruption occurrence depends not only on the details of the plasma state but also on (device-dependent) technical elements of the shot exit scenario. Year-to-year changes in the main disruption causes and a reduction in the disruptivity rate, bound by device and operation upgrades, are reported. Particular trigger instances of DEC (and the full chains when applicable)

[a] See Harrison *et al* 2019 (https://doi.org/10.1088/1741-4326/ab121c) for the MAST Upgrade Team.
[*] Author to whom any correspondence should be addressed.

are shown to occupy different parts of the operation space diagrams, in accordance with prior expectations. Plasma elongation is identified as an important factor influencing details of the chains and its role will be further explored.

Keywords: magnetohydrodynamics, tokamak, disruptions

(Some figures may appear in colour only in the online journal)

1. Introduction

Fast losses of the plasma confinement—disruptions [1]—may threaten future power plant-relevant tokamaks on numerous fronts: through generation of runaway beams piercing the first wall armor [2], deposition of significant thermal and particle loads leading to melting and erosion of the plasma facing components [3] and exertion of substantial electromagnetic forces (resulting from eddy and halo currents) that can compromise the integrity of device structural components [4]. As such, disruptions will have to be mitigated, or ultimately avoided when necessary, in devices such as ITER [5] and SPARC [6].

Previous studies [7, 8] reported on a number of physics and technical instances that causally resulted in plasma disruptions. These instances were later formalized in [9] to 'events' that form a 'disruption event chain' (DEC). A *trigger event* of a DEC for example, an impurity influx and accumulation [10, 11], over/underfueling leading to too high [12, 13] or low plasma density [14] or simply a proximity to known stability limits, creates favorable conditions for destabilization of magnetohydrodynamic (MHD) modes that may cause the disruption through destruction of the confining magnetic flux surfaces. Another possible path to plasma collapse may be through technical issues that are primarily decoupled from the plasma state, such as faults of critical hardware components or faults in the plasma control. Accurate DEC recognition is important: in real-time for deployment of correct actuators preventing disruption and in post-processing to further improve the understanding of disruption root causes, which in return contributes to the development of collapse avoidance strategies.

Independently of the plasma collapse root cause, common disruption elements have been recognized cross-device and cross-shot. Dominant among those are abnormal (deviating from requested) variations in the plasma current I_p and vertical position Z, such as I_p quenches, transient 'spikes' and plasma column vertical displacements [15–17]. Given their close association with disruptions and their common occurrence, they can serve as simple, yet reliable indicators of an upcoming/ongoing plasma collapse.

Origins of I_p and Z anomalies are diverse. Elongated plasmas are naturally unstable to vertical displacements of the plasma column [18] and failure of vertical stabilization may result in unrecoverable vertical displacement events and plasma terminations. Through magnetic stochastization, MHD modes may cause thermal quenches and fast relaxations of the current density profile featuring I_p spikes [19–21]. This phenomenon may be perturbative up to a point of being imminently followed by an I_p decay in highly resistive plasmas, through a quench, until a complete plasma loss. These anomalies are typically among the last events within the full event chain and in principle they may appear in a different order and/or be missing in the DEC, with their appearance being bound to a particular plasma state, plasma control capabilities and machine engineering configuration. As such, despite the fact that they are usually not the primary trigger events, DECs consisting of these anomalies *alone* may reflect the earlier disruptive plasma state evolution and thus can be used to create basic disruption groups defined per trigger events of those reduced DECs. These disruption groups (presented in section 3.3) are coarsely, yet robustly indicative of the driving disruption cause. In addition, a binary disruptive shot classifier may implement recognition of these anomalies. In particular, while I_p spikes and vertical displacements may be generally self-sustained and/or compensated and thus do not lead to an immediate plasma termination, major I_p quenches usually result in irreversible plasma loss. As such, an I_p quench represents a suitable binary indicator of a disruptive plasma, i.e. its detection can serve as a simple, yet fundamentally important classifier of disruptive shots. It is worth noting that a general consensus on the definition of a binary plasma disruption classifier, that would separate disruptive and non-disruptive shots, has not been reached across previous references, for reasons including a clear definition of the current quench severity, and even the lack of technical event considerations in the analysis in certain cases.

The DECAF[6] [9] code aims at tokamak plasma disruption characterization and prediction through its continuously expanding analysis tools and a set of physics-driven modules that capture various elements of the disruptive chains. Besides those, DECAF newly recognizes technical events (such as various hardware and software faults, plasma control system phase changes etc) in its event module fleet. In a fully automated and abstracted manner, it captures the above described I_p and Z anomalies of interest and here the code is used to achieve two goals:

(a) Report on a disruption occurrence indicated by an I_p quench-based disruptive plasma binary classifier. The disruptivity will be discussed in the context of the intentional plasma termination deployment, a key element to

[6] U.S. and international patents pending.

be recognized in any DEC for proper interpretation of the causality of events leading to the plasma collapse.

(b) Explore the statistics of disruption groups defined by trigger events in DECs composed of I_p and Z abnormalities and present the location of the groups in the plasma operation space. The hypothesis is that both the statistics of occurrence and location of DEC trigger events in the operation space are bound to the plasma stability boundaries sensitive to the given DEC, but also to the usual experimental scenario, engineering capabilities and setup.

The two topics combined bring an important insight into the physics and/or engineering elements driving disruptions in a given study set. Hence, a background for further study of disruption root causes and hints for future development of real-time plasma control and termination schemes can be obtained. This study was conducted on a large multi-device (KSTAR, MAST-U and NSTX-U) and multi-year (7 years of operation in total for the three machines) shot database, taking advantage of the capability of the DECAF code to analyze disruptive event chains on large multi-machine datasets in a time-efficient manner. Thanks to this capability, a unique year-to-year improvement in the device operation captured by the DECAF analysis will be reported in the respective paper sections.

This document is organized as follows: details on the multi-device/year study database are provided in section 2. A description of DECAF modules recognizing I_p and Z anomalies can be found in section 3 and the I_p quench-based binary disruptive plasma classifier is described in section 3.2. Disruption groups are defined in section 3.3. Disruption occurrence captured through I_p quench is shown in section 4. Statistics of disruption groups and their locations in the machine operation space are provided and discussed in sections 5.1 and 5.2, respectively. Similar information has been reported for the most frequently occurring full DECs in section 6. A summary of the findings is in section 7.

2. Multi-device and year study database

The database of interest consists of the full KSTAR 2019-2022, MAST-U 2021-2022 (internally called MU01 and MU02) and NSTX-U 2016 campaigns. The corresponding shot ranges, given in table 3, span from the first to the last attempt for a plasma discharge. All shots within these ranges were labeled through a newly implemented DECAF categorization algorithm that discriminates between plasma and no-plasma discharges. Basic discharge categories recognized by DECAF are listed in table 1. In the case of the first four categories, no plasma was achieved during the shot. The categorization feature is one of the supporting elements that allows DECAF to study DECs in full year databases in a time-efficient manner as the analysis is only conducted on plasma shots. On top of that, it provides an extra information about the underlying reason for the no-plasma discharge, a detail that may be of interest for machine operators and future device designers.

Table 1. Criteria for DECAF basic shot categories.

Category	I_p criteria	B_t criteria
No I_p/B_t data	I_p or B_t data missing	
No toroidal field	—	$\lvert\overline{B_t}\rvert < B_{t,vac}$
Vacuum shot	$\lvert\overline{I_p}\rvert < I_{p,vac}$ & $\max(I_p) < I_{p,max}$	$\lvert\overline{B_t}\rvert \geqslant B_{t,vac}$
Failed I_p breakdown	$I_{p,vac} \leqslant \lvert\overline{I_p}\rvert$ & $\max(I_p) < I_{p,bd,max}$ & $I_p(t = \text{time}(I_{p,bd,min})) < I_{p,bd,min}$	$\lvert\overline{B_t}\rvert \geqslant B_{t,vac}$
Plasma shot	Otherwise	

Table 2. Device-dependent thresholds for DECAF basic shot categorization.

Device	KSTAR	MAST-U	NSTX-U
Time range (s)	[0,10]	[0,1.1]	[0,1.1]
$B_{t,vac}$ (T)	0.2	0.1	0.1
$I_{p,vac}$ (MA)	0.05	0.02	0.02
$I_{p,max}$ (MA)	0.05	0.07	0.05
$I_{p,bd,max}$ (MA)	0.3	0.3	0.3
$I_{p,bd,min}$ (MA)	0.1	0.1	0.1
Time($I_{p,bd,min}$) (s)	0.15	0.2	0.15

To categorize a given shot, the mean values of I_p and vacuum magnetic toroidal field on axis B_t are compared to a set of device-dependent thresholds. The thresholds, initially set to educated guesses (through a port of thresholds from a device of similar characteristics, or through an assessment of the expected threshold values based on known device operations and constraints), are iteratively optimized in hundreds to thousands of cases until successful categorization is achieved on the full test set. Thresholds for the set of devices of the hereby interest are listed in table 2. A specific category is assigned to the shot based on fulfillment of criteria for the given category (see table 1). The mean is applied to I_p and B_t signals delimited in duration by device-specific time ranges given in table 2, second row. Shots falling into the no-plasma category have no disruptive events to be recognized and were thus omitted by DECAF in the here presented study. As for the plasma shots, no human deselection was applied on any discharge and all shots were analyzed.

Counting of (no) plasma shots is given in table 3, third column, and in figure 1. Furthermore, to assure completeness of the input for the DEC analysis in disruptive shots (analysis results presented in sections 5 and 6), DECs were further analyzed for plasmas reaching an I_p flat-top phase and shots with I_p and Z measurements acquired up to at least 1 ms after the onset of the I_p quench phase. The final counting of plasma shots fulfilling these conditions is listed in table 3, fourth column.

Table 3. Summary of the study database.

Device & year	Shot range	Plasma shots (%)	Shots analyzed for DECs (#)
KSTAR 2019	21 779–24 081	60.2	1030
KSTAR 2020	24 136–27 382	68.2	1953
KSTAR 2021	27 806–30 435	83.0	2009
KSTAR 2022	30 732–32 768	78.6	1499
MAST-U 2021	43 313–45 513	61.9	1291
MAST-U 2022	46 020–47 174	57.6	377
NSTX-U 2016	202 514–205 433	35.6	557

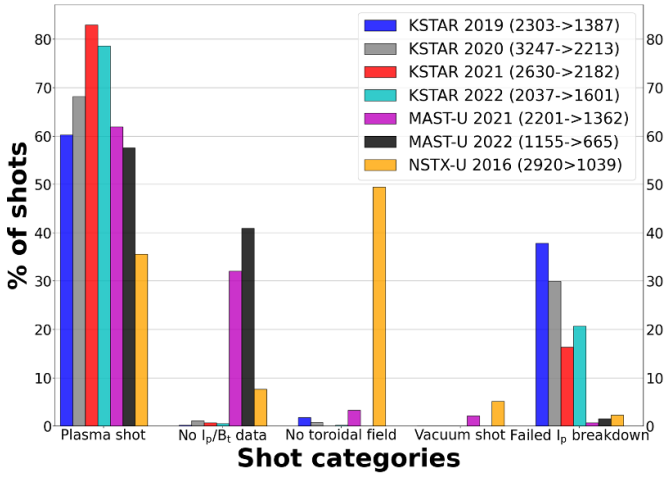

Figure 1. Results of the DECAF shot categorization for the device-experimental year pairs. Shots that passed the I_p breakdown fall into the 'Plasma shot' category (see table 1). Numbers of Total→Plasma shots are indicated in parentheses.

3. I_p and Z anomaly detection in DECAF

The DECAF code recognizes its physics and technical events in a fully automated and abstracted manner cross-shot and cross-device. Modules capturing I_p and Z anomalies of interest are presented in section 3.1. All hereby presented events are summarized in the form of event's short description and its acronym in table 4. Details on I_p quench-based disruptive plasmas binary classifier are given in section 3.2 and a basic disruption classification based on these anomalies is defined in section 3.3.

3.1. Events capturing I_p and Z abnormalities

In healthy and well pre-programmed and controlled plasmas, the experimental I_p signal closely follows the target waveform. Significant deviations between the two may be transient (for example, during an I_p spike), or persist on a longer timescale. In both cases, the Ohmic current drive actuators may counteract them in feedback controlled plasmas, but strong plasma perturbations may eventually exhaust the actuators' capacity, resulting in a disruption onset. DECAF evaluates the deviation within its IPR event (firstly presented in [9]) that indicates that the target plasma current request is no longer being met. The code issues a warning that can achieve three different levels, rising from Level 1 (lowest severity warning) to Level 3 (indicating an imminent disruption). To achieve a given level, the deviation of the target to experimental waveform must surpass a predefined threshold. The three thresholds, different for the devices analyzed in this study, were derived experimentally in a way that maximizes the detection accuracy yet assures low false positive detection rate.

Ensuring plasma vertical stabilization is a primary control task in tokamaks. The failure results in a vertical motion developing on $O(1 \times 10^{-3}$ s) time scale that can potentially result in damage to the device components. DECAF captures the vertical motion of the plasma column and issues a warning of Levels 1–3, in analogy to the procedure described in the previous paragraph. Here, however, three distinct target quantities (all associated with the vertical motion) are monitored and compared to experimentally derived, device-dependent multilevel thresholds. Each of the three individual tests contributes to a total warning 'score' [22] that is then mapped to the Level 1–3 warnings in the DECAF VDE event. The target quantities are the following:

- absolute displacement from the target position;
- absolute vertical velocity;
- product of vertical displacement and velocity.

In this work, DECAF calculates the vertical position and velocity using fast resolved (at 10 kHz sampling rates) data acquired by magnetic probes or flux loops, assuring higher event accuracy compared to previous setup that was using plasma vertical position calculated by the MHD equilibrium code [9]. It is noted that the vertical displacement recognition is decoupled here from the detection of a thermal quench and as such it does not discriminate between resistive and non-resistive (sometimes called 'cold' and 'hot') displacement events.

I_p spikes are commonly associated with magnetic stochastization [19, 20] and thermal collapses. Various MHD modes may lead to these phenomena: modes that are usually not imminently disruptive, for instance plasma core sawtooth [23, 24] and edge localized modes [25], and modes frequently appearing in the disruptive event chains, such as tearing modes [26, 27], external kink modes [28] and others. Major thermal quenches spanning across a significant part of the plasma radius may be followed by an I_p quench phase. Both spikes and quenches are among the most basic transient phenomena to be monitored to evaluate the plasma state proximity to a disruption. DECAF recognizes these transients through a hereby expanded processing of the I_p time derivative that allows examination of finer details of constitutional disruption elements. In particular, it recognizes peaks (positive and negative) in the dI_p/dt signal and associates them with the transients in an optimized manner that avoids false peak recognition. As stated earlier, I_p abnormalities captured by this algorithm do not have to causally lead to an imminent disruption. Therefore, in order for a spike and quench to be associated with the definitive plasma collapse, the latter must be

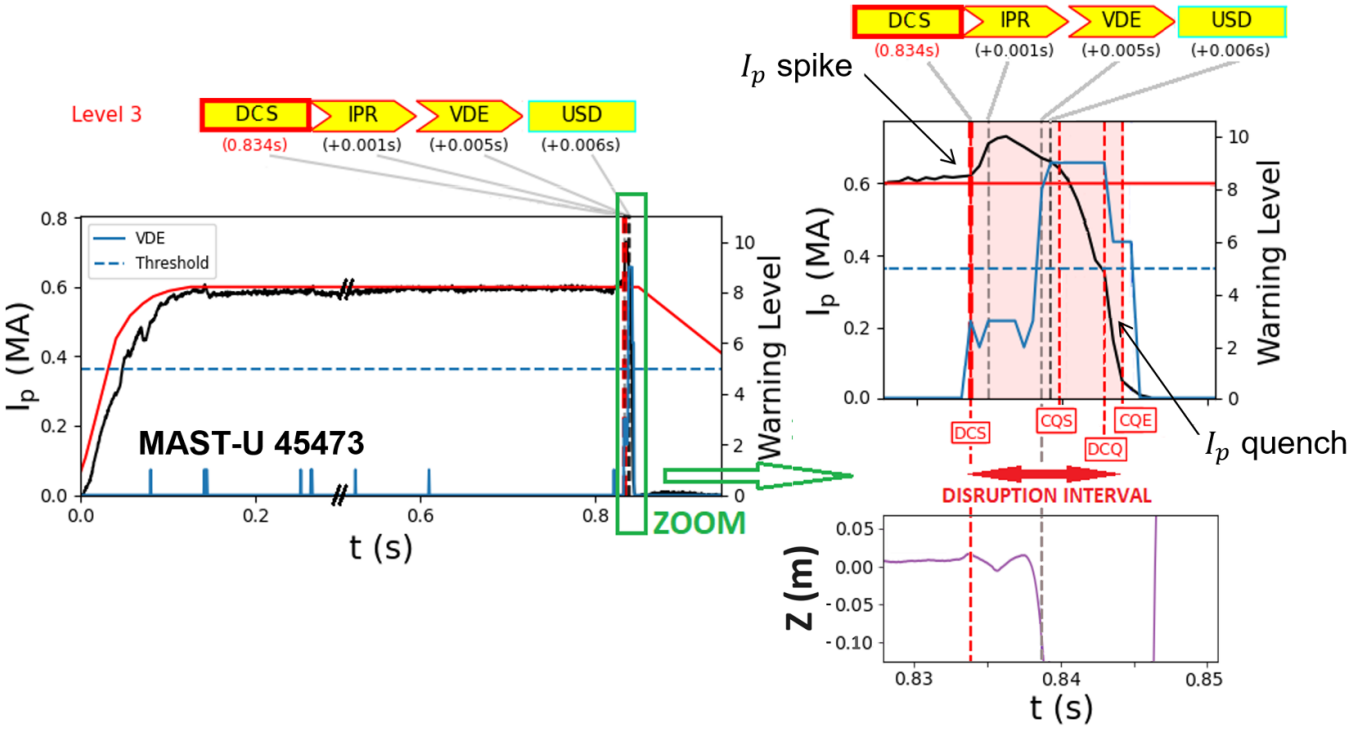

Figure 2. Example of a DEC captured by DECAF in a MAST-U shot 45 473 (left) and a zoom into the disruption interval (upper right) and the vertical displacement (lower right). The chain of consecutive events of interest here is DCS → IPR → VDE → USD → CQS.

recognized in the vicinity of the plasma termination point (I_p falling below a critical threshold set at the order of a couple of % of maximum I_p achieved in the shot) and the former must be imminently followed by a disruptive plasma current quench. These criteria result in DECAF events named disruptive current spike (DCS) and disruptive current quench (DCQ). Given their causal bound to the plasma collapse, these events issue directly a Level 3 warning at the time they are recognized (contrary to the above described multi-level warnings issued by the IPR and VDE events).

It should be noted that the hereby described DCS and DCQ recognition (that uses as an input only the I_p signal) is reserved for shot post-processing. Future implementation of these DECAF events in real-time (that will expand the set of real-time DECAF events already implemented in the KSTAR plasma control system [29]) will require the algorithm for peak recognition in dI_p/dt to be complemented with other important disruption proximity indicators, such as occurrence and extent of thermal quenches, evaluation of disruptive MHD mode amplitude [30, 31], recognition of MHD mode coupling [32] and others.

Figure 2 shows an example of a MAST-U discharge analyzed by DECAF for the above described I_p and Z abnormalities. The Level 3 DEC is initiated by a DCS, a trigger event that is closely followed by an above-threshold deviation of the experimental (black) from the requested (red) I_p waveform captured by the IPR event. A VDE event follows shortly after, as well as USD (engineering Uncontrolled Shut Down technical event, see section 3.3 for more details). In figure 2, a DCS is located at the onset of a *disruption interval*, an interval defining the period of time over which a disruption occurs, which is a far more physically reasonable approach than simply defining the disruption to occur at a single point in time. The interval is an alternative to the disruption time indicator (DECAF event DIS) presented in [9]. Physical events (final collapses of the plasma stored energy, temperature, plasma current etc) are specified in DECAF that set the criteria that define the disruption interval. These criteria are unchanged for a given DECAF model. The advantage of a disruption interval over a singular time is that it can comprise the period of major disruption consequences in terms of heat and particle loads on the plasma facing components, periods of maximum halo and in-vessel induced eddy currents and mechanical forces applied on the vessel (that can reach its peak after full thermal energy content and I_p dissipation [33]). Furthermore, the interval mitigates the ambiguity over the definition of a particular disruption time encountered within the research community. Finally, it allows a simple graphical visualization of distinct disruption elements within the plasma collapse phase and helps to understand the event connection and causality. Figure 2 demonstrates the criteria set for the disruption interval span for the DECAF model applied in this work. As illustrated in the figure, the interval captures a DCQ surrounded by the start and end of the current quench phase (CQS and CQE events, delimiting the negative peak in the dI_p/dt signal associated with the DCQ event) and the DCS that imminently preceded the I_p quench phase.

While the details of the disruption, captured by all of the above introduced DECAF events, are important for disruption dynamics studies, in the following, the focus is on DECs constituted by DCS, IPR, CQS, VDE and USD events (highlighted in bold in table 4). The times at which those events

Table 4. DECAF events of interest (events constituting DECs in this study are highlighted in bold).

DECAF event	Event code
Disruptive current spike	**DCS**
I_p experimental not meeting target	**IPR**
Disruptive current quench	DCQ
I_p quench phase start	**CQS**
I_p quench phase end	CQE
Vertical displacement event	**VDE**
Uncontrolled plasma shut down	**USD**

reach the Level 3 warning determine their order within the DEC. In the example shown in figure 2, the chain of consecutive events of interest is DCS → IPR → VDE → USD → CQS.

3.2. I_p quench-based binary disruption classifier

A robust binary classifier of disruptive and non-disruptive plasmas is a prerequisite for the construction of a plasma shot database serving for any disruption-related analysis. Several commonly occurring disruption elements may be implemented for discrimination of non-/disruptive shots, among which the most frequently considered ones are major vertical movements and thermal and I_p quenches. Each of these three elements suffers from drawbacks in its application as a binary disruptive plasma indicator:

- Thermal and current collapses have been observed in plasmas vertically centered until the full plasma termination [34, 35]. Hence, disruptive shots may be completely missed when relying on vertical displacement detection.
- Thermal quenches develop on millisecond timescales and not all devices are equipped with diagnostics that can resolve them, preventing a universal cross-machine portability of a thermal quench-based classifier. Furthermore, step-wise minor thermal collapses, rather than major singular quenches, and even post-quench recovery of plasma temperature, were reported in devices with metallic first wall armor [8], making the disruption identification somewhat ambiguous without additional DECAF events examining impurity radiation-induced plasma collapses.
- Metal-wall devices were observed to feature slower I_p quenches, frequently accompanied by transient spikes, which makes the quench phase identification technically more challenging. Nevertheless, a major I_p quench leading to a complete plasma loss is in general an irreversible disruption phase, recognized cross-device and cross-shot and documented through basic I_p measurements. Hence, it may be considered as the most suitable universal disruption indicator.

Owing to this universality, DECAF has been expanded to recognize disruptive shots via the detection of the major I_p quench. In the code, the final I_p quench phase is detected through the DCQ event and the quench interval is delimited by CQS and CQE events (defined in section 3.1). Hence, the sequence of DECAF events recognizing the disruptive I_p quench is CQS→DCQ→CQE (see figure 2, upper right), i.e. the first event in the sequence is CQS. Therefore, the I_p quench onset time is given by the time of the CQS event occurrence in the following analysis.

In contrast to disruptive shots, plasmas with I_p ramping down at a (roughly) constant rate do not lead to transients in the dI_p/dt signal (recall section 3.1) and therefore do not trigger the DCQ event. Altogether, discharges without disruptive I_p quench phase cannot have the DCQ, CQS, CQE and DCS events recognized.

It is worth noting that despite the technical challenges described above, recognition of thermal collapses is of primary importance in the context of disruptive event chain analysis, given their key role in the disruption onset. As such, a new fleet of DECAF events, targeting the detection and characterization of thermal quenches and their precursors, is currently under development.

3.3. Basic disruption groups based on I_p and Z abnormalities

The reduced set of DECAF events-of-interest consists of four physics events capturing I_p and Z anomalies and one engineering technical event indicating intentional plasma termination. Combined, a large number of permutations of events (>100) within the DECs may in theory be captured in the study set. The order and appearance (or not) of events within DECs is not random, it is driven by the particular plasma state, off-normal plasma state handling and other factors. While the details of the chains (order and number of events) matter—for example, it allows a detailed understanding of the path that led to the plasma termination—a simple, yet robust disruption classifier can be constructed when the DECs are grouped per trigger event. The onset of trigger events is not random either, it is the result of the plasma state at the time of the trigger event onset that promotes the underlying physics mechanism. As such, trigger events should locate themselves within distinct regions of the plasma parameter space. Knowledge of trigger event location within this space not only helps to further understand the conditions promoting their onset, but it may also help at formulating strategies for deployment of actuators delaying the disruption or completely stabilizing the plasma. Possible driving mechanisms of the trigger events-of-interest (listed in table 4) are the following:

- VDE: meeting of the vertical instability limit within the $\kappa(l_i)$ space (plasma elongation vs. measure of the current profile peaking, the plasma internal inductance), fault of the (active/passive) vertical stabilization;
- IPR: high density limit, in-core impurity accumulation, localized plasma cooling and radiation causing modification of the current profile resulting in experimental I_p not meeting the requested waveform (followed frequently by destabilization of MHD modes);
- DCS: global MHD modes (external ideal kinks, resistive wall modes, born-locked tearing modes etc) disrupting plasma through single I_p spike without prior IPR event;

- CQS: underlying cause to be further studied, with prime candidate being a fast plasma radiative collapse;
- USD: intentional control transition to plasma termination following a detection of fault of critical hardware or software components, proximity to known hardware engineering or plasma stability limits, intentional deployment of massive gas injection etc. Given the rather technical nature of this event, it can in principle be located in any part of the plasma parameter space.

It is noteworthy that the statistical incidence of disruption groups may change over time, for example after an upgrade of critical device hardware and/or software elements [8], major change in the experimental shot planning etc.

4. Disruption recognition via I_p quench detection

Section 3.2 presented the definition of the I_p quench-based classifier of disruptive plasmas implemented in DECAF through the CQS event. Figure 3(*a*) displays the percentage of discharges with CQS recognized by DECAF in the study set consisting of all plasma shots indicated in table 3, third column. While the percentage of CQS in spherical tokamaks MAST-U and NSTX-U is between ∼60%–80%, in KSTAR the percentages approach 100 in all experimental years.

CQS onset must be necessarily viewed in the context of the deployment of the actions leading to the USD event, as the USD may be directly followed by the I_p quench. In the KSTAR case, the USD preceded CQS in [13,11,31,36]% of cases in the years 2019-2022 (see figure 3(*a*)), respectively, indicating that a large number of quenches were induced by other causes than USD. Nevertheless, KSTAR deploys a rather conservative protection of the critical superconducting and other systems. For example, it aims at preventing quenching of its poloidal field coils [36], mitigating damage of the first wall by plasma heating modules etc. These protection schemes are included in the drivers of the USD DECAF event and it can be seen in figure 3(*b*) that prior to KSTAR 2021 this event was mainly deployed at plasma current $I_p \leqslant 0.1$ MA. In the following years, an apparent change in the USD application strategy took place as the USD was deployed also at higher levels of the I_p, up to the point of the flat-top nominal plasma current. The change in the USD deployment strategy led to the fact that it was inducing more I_p quenches.

CQS statistics may be viewed in the context of its onset during the shot phase. CQS occurrences in the I_p flat-top phase (of which an example is shown in figure 2) are indicated in figure 3(*a*). To qualify as a CQS in the flat-top, I_p at the time of the CQS event could not be below 90% of the nominal target I_p flat-top level set by the device operator. It can be seen that the majority of CQS events are initiated in the I_p dynamic phases of the discharge, i.e. outside of the flat-top phase. Empirically, the non-flat-top disruptions happen in the I_p ramp-down phase, indicating significant room for optimization of the shot termination sequence with respect to the prevention of the disruption

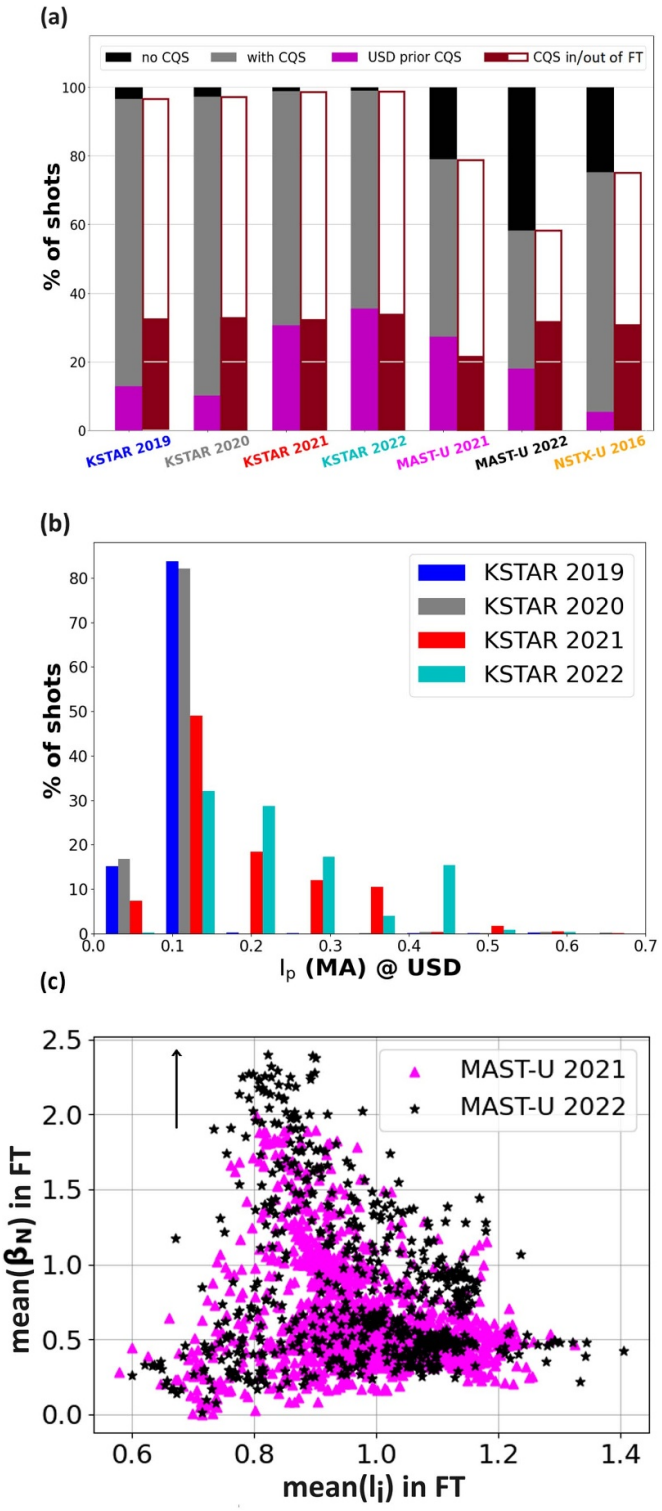

Figure 3. (*a*) Statistics of automatic DECAF recognition of I_p quench phase through the CQS event in the full study database. CQS preceded by the USD are indicated, as well as CQS events happening during or outside of the I_p flat-top (FT) phase. (*b*) Distributions of I_p calculated at the USD event time in KSTAR 2019–2022. (*c*) Stability diagram $\beta_N(l_i)$ in the form of mean values of the quantities calculated during the I_p flat-top phase, MAST-U 2021 and 2022 datasets. Shift towards higher mean(β_N) values in MAST-U 2022 is indicated by an arrow.

onset (an example of a shot termination improvement leading to decrease in the disruptivity in the plasma ramp-down is discussed below for the MAST-U case).

Generally, upgrades of device components and shot sequence plans may lead to prevention of the disruption and thus reduction of the disruptivity rate. For example, when compared to MAST-U 2021, the MAST-U 2022 set shows a significant decrease (by $\sim$20%) of the discharges with CQS and far fewer disruptions in the plasma I_p ramp-down, which may be at least partly attributed to the year-to-year improvement of the plasma shape and vertical stability controllers [37]. On the other hand, the rate of flat-top disruptions increased in MAST-U 2022 compared to MAST-U 2021. This may be attributed to the overall higher plasma performance in MAST-U 2022 compared to the 2021 campaign, demonstrated in figure 3(*c*) that compares the campaign's data points within a $\beta_N(l_i)$ (β_N is the normalized ratio of kinetic to magnetic pressure and l_i the normalized plasma internal inductance) stability diagram (the data points correspond to mean values of the quantities calculated during the I_p flat-top phase). In MAST-U 2022, the mean β_N in flat-top was overall higher than in 2021, making the plasma more vulnerable to destabilization of MHD modes which could in turn disrupt the plasma.

It is necessary to stress that once the I_p completes the pre-programmed flat-top phase, the device operators may set to automatically switch off active control of critical plasma parameters. Frequently, this may result in a plasma disruption, contributing thus to the CQS event occurrence. In current machines, the disruptions pose a rather minor risk to the machine components, but with the transition to reactor-relevant devices and plasmas, this procedure may generally no longer be applicable.

5. DEC trigger event statistics and location in plasma operation space

Section 3.3 introduced basic disruption groups according to the here studied DECAF events capturing I_p and Z abnormalities. In the following, statistics of the basic disruption groups in the study set will be presented (section 5.1), followed by examples of DEC trigger event locations in the machine operation diagrams (section 5.2). Both points expand the analysis of DECAF events presented in [9] in that here, the focus is on the analysis of the DEC triggers and the plasma state at the trigger event times.

5.1. Statistics of disruption groups in the study database

Figure 4 shows the occurrence (in %) of DECs trigger events in the study database identified by DECAF. The percentage of VDEs as trigger events has reduced over the years in KSTAR, indicating a change of strategy in prevention of this type of instability. Furthermore, the USD evolves as an important trigger event over time, complementing the observations of the USD deployment presented in section 4. In the MAST-U case, the IPR trigger event appears to have been suppressed at the expense of the DCS event, possibly because of an inclination to destabilization of different type of MHD instabilities in the second year of the device operation. Percentage of other events stayed approximately the same from year-to-year, yet it should be stressed that the overall disruptivity rate decreased in MAST-U 2022 compared to MAST-U 2021 (recall section 4). Finally, in the case of the NSTX-U 2016, IPR, VDE and DCS were identified at roughly similar percentages, with IPR being the most frequent trigger event.

5.2. Location of DEC trigger events in plasma operation diagrams

As introduced in section 3.3, distinct DECs grouped per trigger event may be located in different parts of the device operation space and stability diagrams as they reflect distinct causes leading to their onset. The global plasma parameters usually examined in the context of MHD mode destabilization are plasma shape parameters (plasma triangularity δ and elongation κ), β_N, l_i, Greenwald density fraction f_{GW}, safety factor at the 95% of the toroidal flux q_{95} and others. The location of DEC trigger events in various operation and stability diagrams was examined here for all device and year database pairs, and the most prominent clustering of the disruption groups was recognized in diagrams constituted by q_{95}, l_i and κ parameters. In the following, selected diagrams for a representative part of the database are shown and discussed. Plasma parameters in the diagrams were calculated at the time of the DECAF event reaching the Level 3 warning levels (recall figure 2). USD and CQS events data points are not shown in the plots. USD is a technical event that can be in principle located in any part of the diagrams and CQS as a trigger event needs further investigation of the disruption root cause prior to any discussion related to its position in the stability diagrams (given its overall low occurrence in the data set, its position in the diagrams does not provide useful hints on the driving cause).

Figure 5, upper plots, display three selected diagrams for the MAST-U 2021 database [38]. The DCS trigger event is clustered in the $l_i(q_{95})$ diagram (left) at the stability boundary that was previously observed in [34] in the full-tungsten ASDEX-U device for the high plasma density limit disruptions. A significant fraction of the IPR events are located in broader current density profiles (i.e. at lower l_i). Broader current density profiles might be inclined to the growth of external kinks in various mode structures (along the q_{95} line). Furthermore, DCS trigger events tend to be located in the highest elongated plasmas for a given l_i where VDE events are expected ($\kappa(l_i)$, middle) and in the $l_i/q_{95}(\kappa)$ diagram (right) the DCS trigger events are found at the highest values of the ratio for a given κ, with l_i/q_{95} being a proxy for the free energy driving the growth of MHD modes [39]. Note that the VDE points are roughly homogeneously distributed in the $l_i(q_{95})$ and $\kappa(l_i)$, contrary to usual expectations. A year-to-year upgrade of the plasma shape controller and improvements in maintaining the radial field balance led to the apparent elimination of VDEs destabilized in plasmas with magnetic axis localized radially closer to the central solenoid (figure 5,

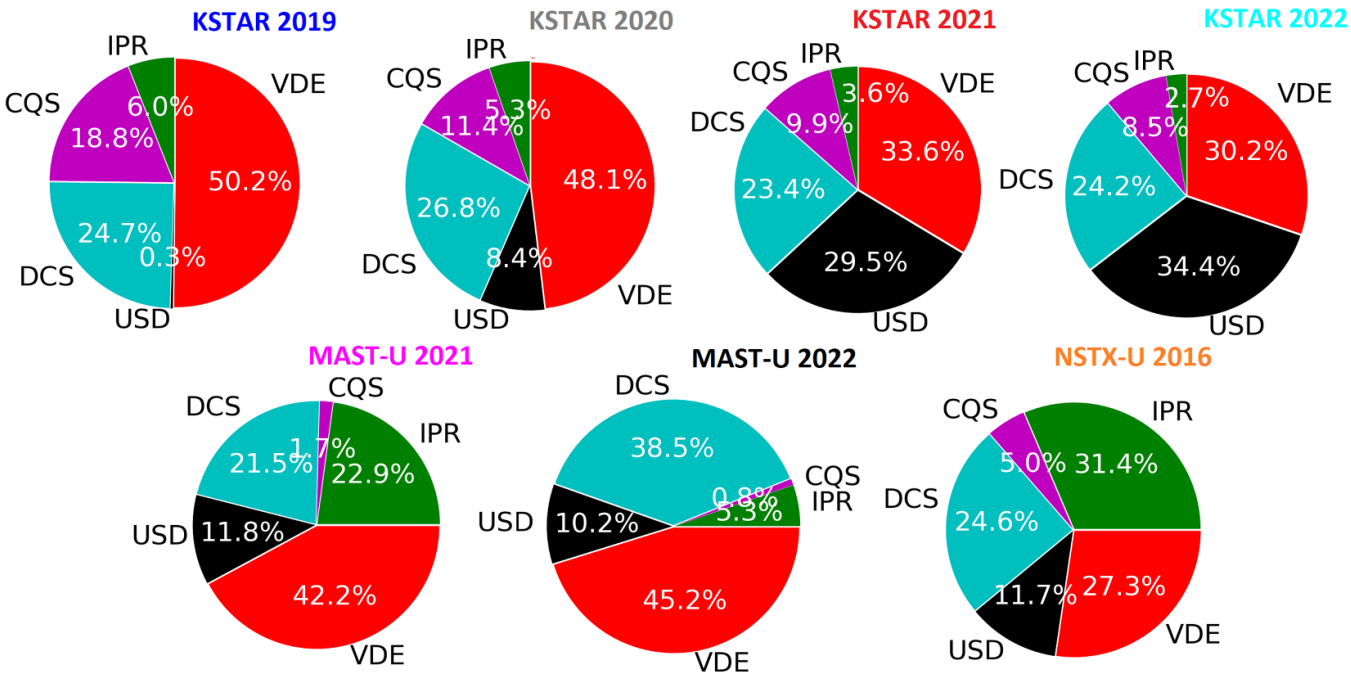

Figure 4. Percentage of all DECs grouped per trigger event in the study set.

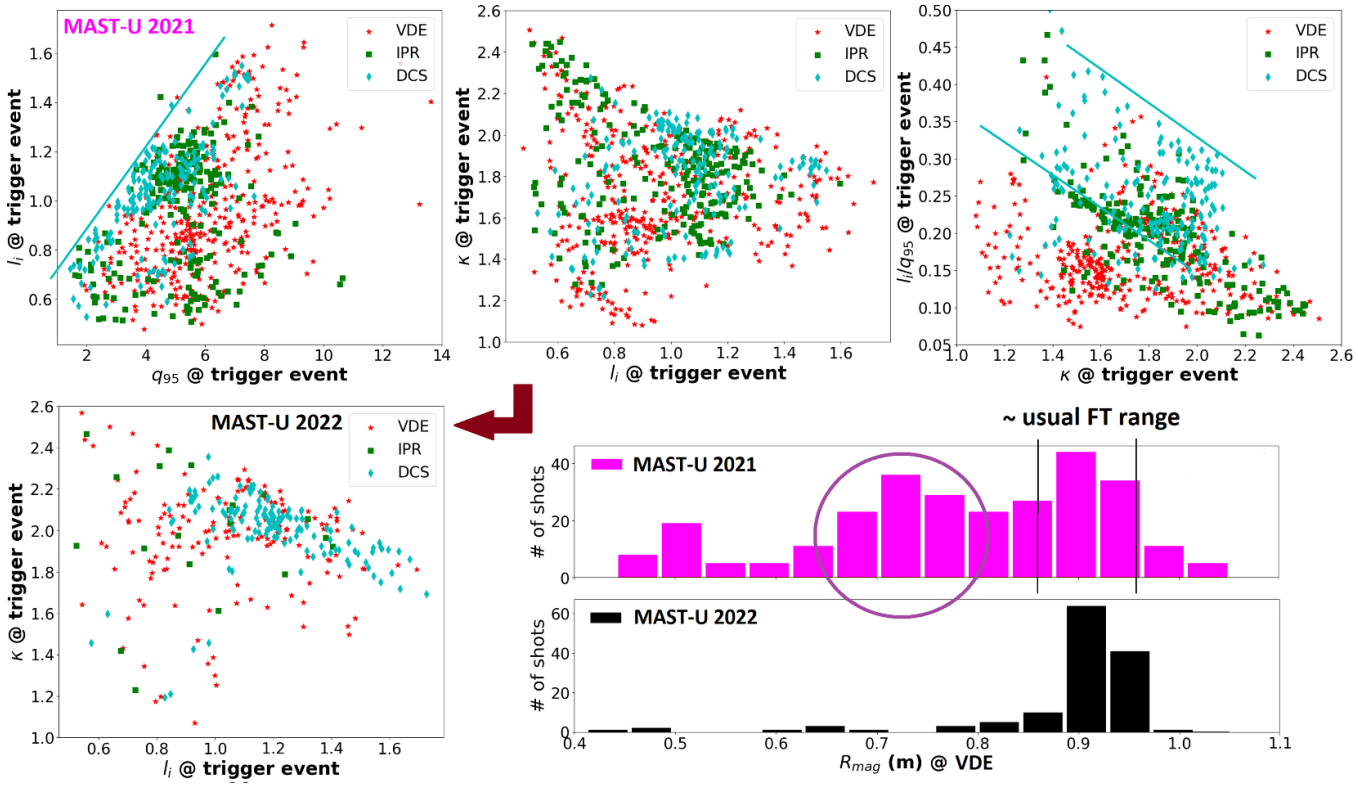

Figure 5. Upper plots and lower left: trigger events occurrence in selected operation space diagrams, MAST-U 2021-22. Lower right: radial position of the magnetic axis R_{mag} calculated at the time of the VDE event in MAST-U 2021-22.

lower right, encircled), usually destabilized in the early I_{p} flat-top phase. This elimination probably contributed to the overall reduction of the disruptivity rate (discussed in section 4) and clearance of the VDE points in the central part of the $\kappa(l_i)$ diagram.

Figures 6(*a*) and (*b*) display $\kappa(l_i)$ diagrams for the KSTAR 2022 and NSTX-U 2016 sets [40], respectively. The clustering of the three trigger events of interest is recognizable in the NSTX-U case, with a clear separation of the IPR data points (located at an overall lower plasma elongation) from

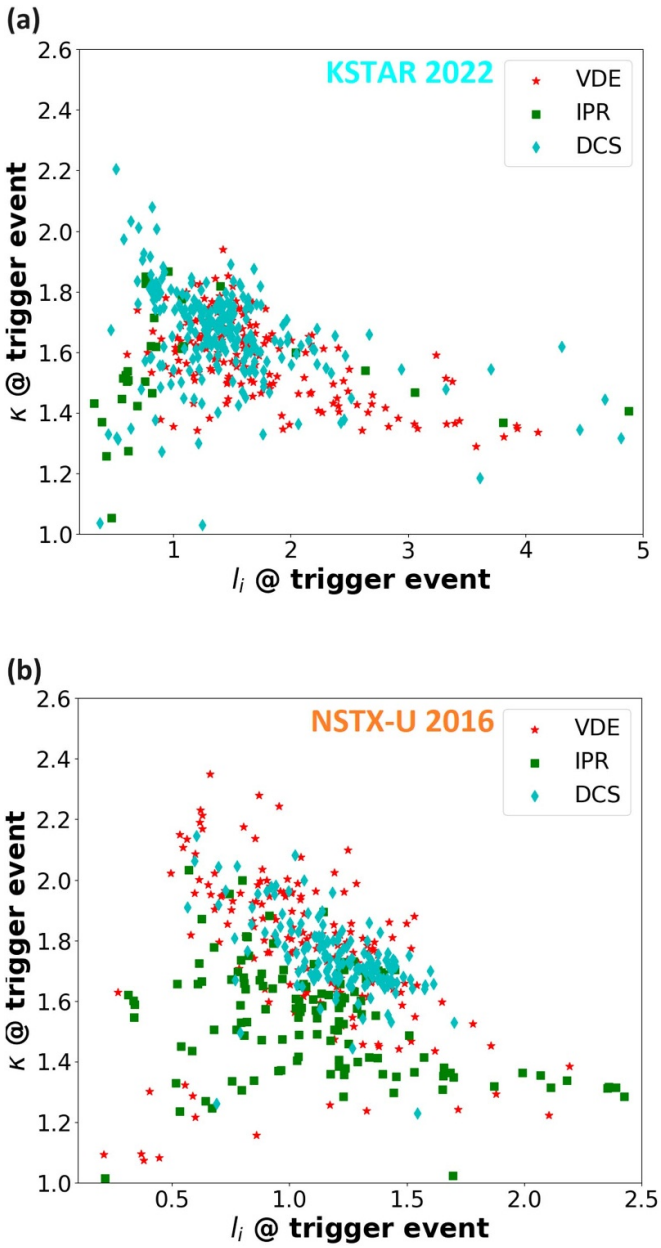

Figure 6. Trigger events occurrence in the $\kappa(l_i)$ diagram in KSTAR 2022 (*a*) and NSTX-U 2016 (*b*).

the other events. The predominant location of the VDE and DCS events is close to the upper stability boundary. In the case of KSTAR 2022, clustering of the disruption groups is not so distinct. In other KSTAR experimental years, the trend is similar.

A multi-device $l_i(q_{95})$ diagram shown in figure 7 displays DCS trigger event points for four selected device-year databases. While in the case of KSTAR 2022 the points are approximately restricted to the $q_{95} \sim$ 3–6 region, points along the l_i are roughly unrestricted. The situation is clearly reversed in the MAST-U case with a year-to-year reduction of points below $q_{95} \sim 4.8$. Further investigation found that a substantial part of MAST-U 2021 points located below this limit were acquired

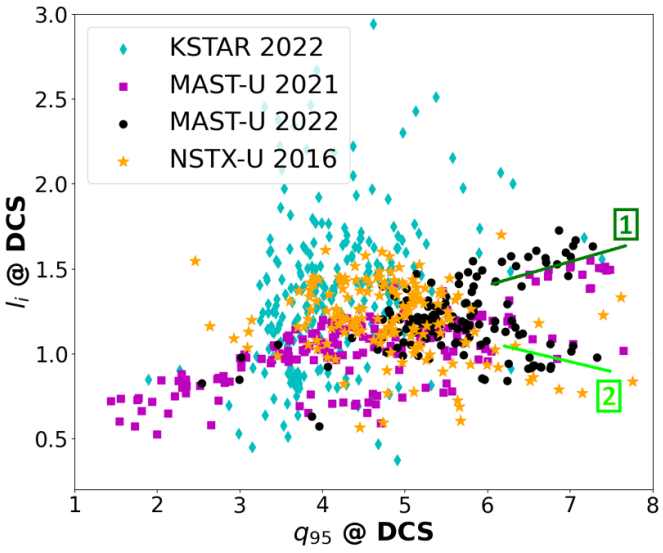

Figure 7. Multi-device location of the DCS trigger event in the $l_i(q_{95})$ diagram. Two distinguishable branches of MHD instabilities (MAST-U case) are highlighted in green color.

during the initial phase of the experimental year, following the restart of the machine after the major upgrade of the former MAST device to MAST Upgrade. The progressive development of a stable flat-top scenario and beyond (bound with tailoring of the stable current profile and other elements) contributed to the reduction of the DCS trigger event points in this part of the diagram.

Interestingly, two branches of DCS trigger points can be recognized in both MAST-U experimental years. The two branches (visualized in figure 7 with green lines) are separated along the l_i axis into two regions, with the internal inductance being roughly restricted to $l_i \sim$ [1.5,1.7] (branch 1) and $l_i \sim$ [0.8,1.2] (branch 2). The region in between the branches is free of DCS events for $q_{95} \gtrsim 6.3$. Figure 8(*a*) reduces figure 7 to the MAST-U 2022 data set. There, the two branches are separated in the (l_i,q_{95}) space by the following limits: 1 $l_i >$ 1.28; 2 $l_i < 1.28$ and $q_{95} > 4.4$ (to eliminate outliers located below $q_{95} < 4.4$). Through those limits, branches 1 and 2 contain 41 and 88 data points, respectively. Figure 8(*b*) displays histograms of the plasma durations of shots falling into the two groups. Shots with the longest durations ($\geqslant 0.75$ s) are predominantly located in branch 1. Plasmas of this duration represent a minority in branch 2. This branch also contains short plasmas disrupted in the early flat-top phase (maximum duration of ~ 0.3 s). An assessment of the performance of plasmas belonging to the two groups was made by calculating the mean value of the β_N during the I_p flat-top phase. Next, the median values of the 41 and 88 mean($\beta_{N,\text{flat-top}}$) values were calculated. The resulting median values were $\beta_N = 0.83$ and $\beta_N = 0.60$ for branches 1 and 2, respectively, suggesting that plasmas within branch 1 tended to have the onset of disruptive MHD instabilities delayed and achieved better plasma performance.

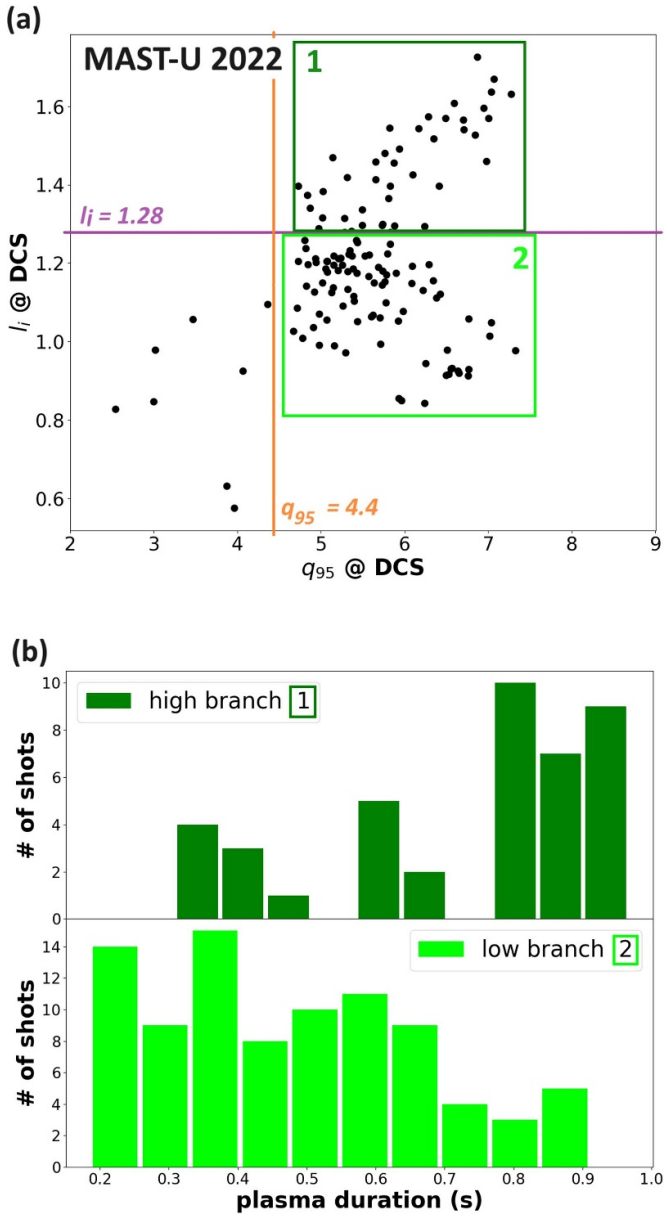

Figure 8. (*a*) Location of the DCS trigger event in the $l_i(q_{95})$ diagram for the MAST-U 2022 database. The two branches of $l_i(q_{95})$ points (delimited by the l_i and q_{95} limits visualized by magenta and orange lines) are highlighted in green colors. (*b*) Plasma durations (in seconds) of shots belonging into the two branches.

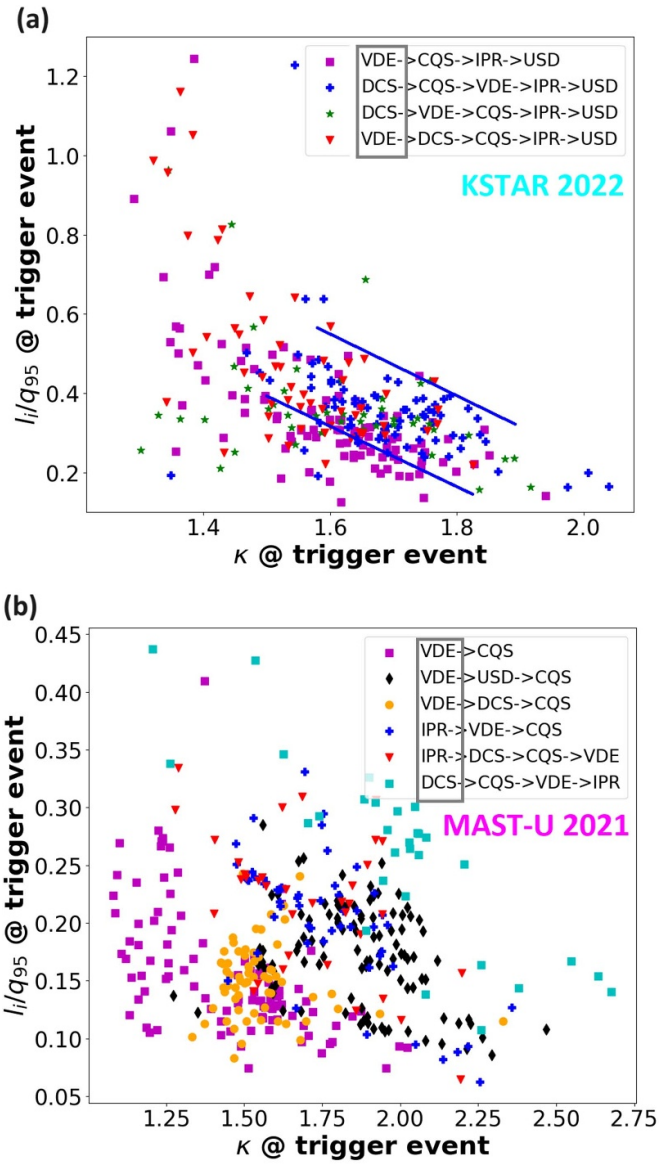

Figure 9. Location of dominant DECs in the $l_i/q_{95}(\kappa)$ diagram: (*a*) KSTAR 2022, (*b*) MAST-U 2021. DEC trigger events are highlighted by a gray rectangle.

6. Dominant DEC location in $l_i/q_{95}(\kappa)$ operation diagram

The order and appearance (or not) of events within DECs depend on the particular plasma state evolving under the influence of both internal and external factors. In principle, not just the single trigger events, but also common chains may be separated within the operation space diagrams. Figure 9 tests this hypothesis in the $l_i/q_{95}(\kappa)$ diagram (data points calculated at the time of the trigger event) for the most frequent (representing in total at least ~45 % of all DECs) disruptive event chains for device databases that have sufficient statistical set for the study (here KSTAR 2022 and MAST-U 2021). It can be seen that the most frequent DECs initiated by DCS are located along the upper $l_i/q_{95}(\kappa)$ boundary, roughly separated (yet still intermixed for lower l_i/q_{95} values) from VDE-triggered DECs in the KSTAR 2022 case. The MAST-U DECs appear in clear clusters in the diagram and κ seems to be an important factor in the appearance of events within DECs. For example, in the VDE trigger event case in the first and third chains (listed in the plot legend), the DCS only appears in the chain for $\kappa \gtrsim 1.45$.

7. Summary and outlook

Unmitigated plasma collapse will have to be avoided in power plant-relevant fusion devices and beyond. The tokamak

research community recognizes the ultimate importance of understanding the disruption root causes and elements of disruptive event chains and a significant effort is invested in the development of collapse avoidance strategies.

Abnormal development of the plasma current and vertical position will have to be monitored in next-step tokamaks due to their critical role in the disruption onset. Here, the occurrence of disruptions was explored via the detection of an I_p quench and exploration of disruptive event chains, constituted by these abnormalities, was reported for in total seven full device-years pairs of operation of three machines. The DECAF code, equipped with new physics and technical event modules and analysis tools was used for this purpose. It was shown that the disruption occurrence captured through the I_p quench depended not only on the details of the plasma state, but also on (device-dependent) technical details of the shot exit scenario. Year-to-year changes in main disruption triggers and even a reduction in the disruptivity rate, bound to device and operation upgrades, were reported. Particular trigger instances of disruptive event chains (and the full chains, when applicable) were shown to occupy predominantly distinct parts of the operation space diagrams, in accordance with a prior expectation. Plasma elongation has been identified as an important factor influencing triggers and details of the disruptive event chains and its role in them will be further investigated.

The analysis presented hereby utilizes a subset of DECAF code events capturing basic disruption elements and explores their application for the purposes of binary disruptive plasma classification and basic disruption categorization. The number of events and the level of detail of disruption dynamics and characterization captured by these events allowed us to identify the main disruption cause patterns and to follow year-to-year major collapse cause evolution. Further expansion of the analysis, through inclusion of existing and new DECAF event modules (among which the most imminent ones to be implemented focus on recognition of thermal quenches and characterization of their driving MHD precursors) will provide more details on collapse driving causes, fragment the here presented disruption groups into finer segments and add new elements into the disruptive event chains. This increase of the disruption grouping and chain 'resolution' is undoubtedly desirable for further understanding of the physics mechanisms driving the disruption precursors and tailoring of the collapse avoidance techniques. At the same time, the lightweight analysis presented in sections 5 and 6 will eventually saturate and more advanced automated analysis techniques of collapse triggers and disruptive event chains will have to be applied.

Deployment of forecasters of major disruption precursors is a key, and continuously expanding capability of the DECAF code. The here presented data on the frequent occurrence of vertical displacement events such as disruption triggers across machines and years of operation support the ongoing implementation of a VDE forecaster based on the vertical stability criterion formulated by Leuer [41]. A real-time implementation of the VDE forecaster is foreseen in the upcoming KSTAR and MAST-U experimental campaigns. Ultimately, the forecaster will be coupled to an actuation of the disruption avoidance and/or mitigation action, a capability that has a precedent in the DECAF MHD mode locking forecaster that was successfully deployed in real-time during the KSTAR 2022 campaign [29].

Finally, the presented paper reports on the statistics of the disruption occurrences and does not categorize disruptions based on their severity. A new capability of the DECAF code, currently under development, will evaluate criteria that discriminate between disruptions that require mitigation and 'benign' disruptions, i.e. plasma collapses whose consequences can be inherently sustained by the device components and design. This level of disruption classification is of the utmost interest in devices in which the mitigation action is highly perturbative to the subsequent device operation (such as ITER) and is thus meant to be deployed only under the risk of device damage due to unmitigated plasma collapse.

Acknowledgment

This work has been supported by US DOE Grants DE SC0020415, DE SC0021311, DE SC0018623, DE AC02 09CH11466 and (part –) funded by the EPSRC Energy Programme (Grant No. EP/W006839/1).

This work was also supported by the R&D Program of 'KSTAR Experimental Collaboration and Fusion Plasma Research' (EN2301-14) through the Korea Institute of Fusion Energy (KFE) funded by Korea Ministry of Science and ICT (MSIT).

This work has been carried out within the framework of the EUROfusion Consortium, funded by the European Union via the Euratom Research and Training Programme (Grant Agreement No. 101052200–EUROfusion). Views and opinions expressed are however those of the author(s) only and do not necessarily reflect those of the European Union or the European Commission. Neither the European Union nor the European Commission can be held responsible for them.

The digital data for this paper can be found in https://doi.org/10.34770/h0p3-qq80.

ORCID iDs

V. Zamkovska https://orcid.org/0000-0001-8437-4576
M. Tobin https://orcid.org/0000-0003-2276-6448
J.W. Berkery https://orcid.org/0000-0002-8062-3210
Y.S. Park https://orcid.org/0000-0001-8815-2962
J. Butt https://orcid.org/0000-0002-3322-6060
K.D. Lee https://orcid.org/0009-0007-0480-5358
C.J. Ham https://orcid.org/0000-0001-9190-8310

References

[1] Schuller F.C. *et al* 1995 *Plasma Phys. Control. Fusion* **37** A135–62

[2] Breizman B.N., Aleynikov P., Hollmann E.M. and Lehnen M. 2019 *Nucl. Fusion* **59** 083001
[3] Ueda Y., Coenen J.W., De Temmerman G., Doerner R.P., Linke J., Philipps V. and Tsitrone E. 2014 *Nucl. Fusion* **89** 901–6
[4] Sadakov S., Furmanek A., Calcagno B., Bertolini C., Khomiakov S., Kolganov V. and Poddubnyi I. 2015 *Fusion Eng. Des.* **98–99** 1601–4
[5] Lehnen M. *et al* 2015 *J. Nucl. Mater.* **463** 39–48
[6] Sweeney R. *et al* 2020 *J. Plasma Phys.* **86** 865860507
[7] de Vries P.C., Johnson M.F., Alper B., Buratti P., Hender T.C., Koslowski H.R. and Riccardo V. 2011 *Nucl. Fusion* **51** 053018
[8] de Vries P.C. *et al* 2012 *Plasma Phys. Control. Fusion* **54** 124032
[9] Sabbagh S.A. *et al* 2023 *Phys. Plasmas* **30** 111945
[10] Rice J., Marmar E.S., Lipschultz B. and Terry J.L. 2011 *Nucl. Fusion* **24** 329
[11] Tokar M.Z., Rapp J., Bertschinger G., Konen L., Koslowski H.R., Kramer-Flacken A., Philipps V., Samm U. and Unterberg B. 1997 *Nucl. Fusion* **37** 1691
[12] Fredrickson E.D. *et al* 1993 *Nucl. Fusion* **33** 141
[13] Berkery J.W. *et al* 2023 *Plasma Phys. Control. Fusion* **65** 095003
[14] Haye R.J.L. *et al* 1992 *Phys. Fluids* B **4** 2098
[15] Pau A. *et al* 2017 *Fusion Eng. Des.* **30** 111945
[16] Atanasiu C.V. *et al* 2019 *J. Phys.: Conf. Ser.* **1391** 012123
[17] Myers C.E., Eidietis N.W., Gerasimov S.N., Gerhardt S.P., Granetz R.S., Hender T.C. and Pautasso G. 2017 *Nucl. Fusion* **58** 016050
[18] Park W., Belova E.V., Fu G.Y., Tang X.Z., Strauss H.R. and Sugiyama L.E. 1999 *Phys. Plasmas* **6** 1796
[19] Nardon E., Särkimäki K., Artola F.J. and Sadouni S. (the JOREK team and JET Contributors) 2023 *Nucl. Fusion* **63** 056001
[20] Wesson J. 2011 *Tokamaks* (Oxford University Press)
[21] Boozer A.H. 1996 *Phys. Plasmas* **27** 102305
[22] Gerhardt S.P. *et al* 2013 *Nucl. Fusion* **53** 063021
[23] McGuire K. and Robinson D.C. 1979 *Nucl. Fusion* **19** 505
[24] Jardin S.C., Krebs I. and Ferraro N. 2020 *Phys. Plasmas* **27** 032509
[25] Zohm H. 1996 *Plasma Phys. Control. Fusion* **38** 105
[26] Rutherford P. 1981 *Physics of Plasmas Close to Thermonuclear Conditions* (Pergamon)
[27] Buttery R.J. *et al* 2000 *Plasma Phys. Control. Fusion* **42** B61–B73
[28] Lee J.K. 1986 *Nucl. Fusion* **26** 955
[29] Sabbagh S.A. *et al* 2023 High accuracy, multi-device physics-based tokamak disruption prediction and forecasting with first real-time demonstration *Proc. 29th IAEA Fusion Energy Conf.* p /7 2038
[30] Klevarova V., Zohm H., Pautasso G., Tardini G., McDermott R., Verdoolaege G., Snipes J., Vries P.C.d. and Lehnen M. 2020 *Plasma Phys. Control. Fusion* **62** 025024
[31] de Vries P.C. *et al* 2016 *Nucl. Fusion* **56** 026007
[32] Suttrop W. *et al* 1997 *Nucl. Fusion* **37** 119
[33] Artola F.J., Loarte A., Hoelzl M., Lehnen M. and Schwarz N. (the JOREK Team) 2022 *Nucl. Fusion* **62** 056023
[34] Klevarova V. *et al* 2020 *Fusion Eng. Des.* **160** 901–6
[35] Pautasso G., Giannone L., Gruber O., Herrmann A., Maraschek M. and Schuhbeck K.H. 2011 *Nucl. Fusion* **51** 043010
[36] Hahn S.-H. *et al* 2020 *Fusion Eng. Des.* **156** 111622
[37] Private communication with G. Cunningham
[38] Berkery J.W., Sabbagh S.A., Kogan L., Gibson S., Ryan D., Zamkovska V., Butt J., Harrison J. and Henderson S. 2023 *Plasma Phys. Control. Fusion* **65** 045001
[39] Sweeney R., Choi W., La Haye R.J., Mao S., Olofsson K.E.J. and Volpe F.A. 2017 *Nucl. Fusion* **57** 016019
[40] Berkery J.W. *et al* 2024 *Nucl. Fusion* (https://doi.org/10.1088/1741-4326/ad3092)
[41] Tobin M. *et al* 2024 Vertical instability forecasting and controllability assessment of multi-device tokamak plasmas in DECAF with data-driven optimization *Plasma Phys. Control. Fusion* submitted